OXFORD

ORIGINAL ARTICLE

Urogenital development in Pallister–Hall syndrome is disrupted in a cell-lineage-specific manner by constitutive expression of GLI3 repressor

Joshua Blake[1,3], Di Hu[1], Jason E. Cain[1,†] and Norman D. Rosenblum[1,2,3,*]

[1]Program in Developmental and Stem Cell Biology, [2]Division of Nephrology, The Hospital for Sick Children, Toronto, Ontario, Canada and [3]Department of Physiology, University of Toronto, Toronto, Ontario, Canada

*To whom correspondence should be addressed at: The Hospital for Sick Children, Peter Gilgan Centre for Research and Learning, 686 Bay Street, Toronto, ON, Canada M5G 0A4. Tel: +1 416 813 5667; Fax: +1 416 813 5252; Email: norman.rosenblum@sickkids.ca

Abstract

Pallister–Hall syndrome (PHS) is a rare disorder caused by mutations in *GLI3* that produce a transcriptional repressor (GLI3R). Individuals with PHS present with a variably penetrant variety of urogenital system malformations, including renal aplasia or hypoplasia, hydroureter, hydronephrosis or a common urogenital sinus. The embryologic mechanisms controlled by GLI3R that result in these pathologic phenotypes are undefined. We demonstrate that germline expression of GLI3R causes renal hypoplasia, associated with decreased nephron number, and hydroureter and hydronephrosis, caused by blind-ending ureters. Mice with obligate GLI3R expression also displayed duplication of the ureters that was caused by aberrant common nephric duct patterning and ureteric stalk outgrowth. These developmental abnormalities are associated with suppressed Hedgehog signaling activity in the cloaca and adjacent vesicular mesenchyme. Mice with conditional expression of GLI3R were utilized to identify lineage-specific effects of GLI3R. In the ureteric bud, GLI3R expression decreased branching morphogenesis. In *Six2*-positive nephrogenic progenitors, GLI3R decreased progenitor cell proliferation reducing the number of nephrogenic precursor structures. Using mutant mice with *Gli3R* and *Gli3* null alleles, we demonstrate that urogenital system patterning and development is controlled by the levels of GLI3R and not by an absence of full-length GLI3. We conclude that the urogenital system phenotypes observed in PHS are caused by GLI3R-dependent perturbations in nephric duct patterning, renal branching morphogenesis and nephrogenic progenitor self-renewal.

Introduction

Pallister–Hall syndrome (PHS) (OMIM# 146510) is a rare autosomal dominant disorder characterized by hypothalamic harmatoma, polydactyly, imperforate anus and urogenital defects (1–7). PHS is caused by genetic mutations that alter the coding sequence of the middle-third of the transcription factor GLI3 (6). Mutations outside of this region cause a related but distinct disorder named Greigs cephalopolysyndactyly syndrome (GCPS) (OMIM# 175700) (8). Urogenital malformations in PHS include renal aplasia, renal hypoplasia, vesicoureteral reflux, hydroureter and a common urogenital opening. The frequency and penetrance of each of these abnormalities is variable but has not been precisely defined (2,3,8,9). GLI3 can act as a transcriptional activator or repressor and is dependent upon the state of Hedgehog (HH) signaling. Frameshift, insertional or point mutations found in PHS cases produce a peptide product that acts as an obligate transcriptional repressor (GLI3R) with varying degrees of activity and phenotypic severity (1–3,8). It is suggested that PHS is caused by increased GLI3-dependent transcriptional repression and not a lack of transcriptional activation that ultimately disrupts a

domain of HH signaling during embryogenesis (1). In the context of urogenital system development, HH signaling and the effects of GLI3R are not well defined.

Mouse models have provided a basis for understanding the embryologic origins of PHS phenotypes and implicated HH signaling in the normal development of the kidney (10–14). Our lab has previously demonstrated that the loss of *Shh*, a ligand of the HH signaling pathway, causes renal agenesis or a single ectopic dysplastic kidney along the dorsal body wall (12). When *Gli3* is genetically removed in a $Shh^{-/-}$ background, kidney induction is restored, suggesting that GLI3R controls ureteric induction (12). We have also demonstrated that ectopic activation of HH signaling disrupts ureteric branching morphogenesis by inhibiting RET–WNT11 signaling in a GLI3R-dependent fashion (15). Moreover, HH signaling activity in the periureteric mesenchyme is required for the differentiation of periureteric smooth muscle and urinary pacemaker cells that mediate urinary peristalsis (11,14,16). While these findings show that GLI3R is pathogenic in the context of altered upstream HH signaling effectors, the ligand-independent effects of GLI3R during kidney development have not been elucidated.

Here, we define a role for GLI3R in controlling kidney size through branching morphogenesis and nephrogenesis, and patterning of the urogenital sinus using mouse models of PHS [the $Gli3^{\Delta699}$ allele (10), and the conditional $Rosa26^{Gli3TFLAG}$ allele (17)]. Moreover, we demonstrate a domain of HH signaling in the nascent urogenital system that is disrupted by GLI3R. Finally, we demonstrate that urogenital system development in the context of PHS is dependent upon the levels of GLI3 repression and not a loss of GLI3 activation.

Results

Obligate GLI3R expression causes a complex urogenital system phenotype

We investigated mechanisms by which GLI3R disrupts murine kidney development by initially analyzing the embryonic phenotype of $Gli3^{\Delta699/\Delta699}$ mutant embryos at E18.5. All mutant embryos were characterized by marked hydroureter (Fig. 1A′ and A″), hydronephrosis (Fig. 1A′, A″, B′ and B″) and a thin renal cortex (Fig. 1B′ and B″). Two additional renal phenotypes were observed: (i) renal hypoplasia ($n = 4/7$, Fig. 1A′) and (ii) a bi-lobed kidney with a single ureter ($n = 3/7$, Fig. 1A″ and B″). In contrast, no abnormalities were observed in $Gli3^{+/+}$ or $Gli3^{\Delta699/+}$ embryos (Fig. 1A and B). Collecting system dilatation was absent in $Gli3^{\Delta699/\Delta699}$ embryos at E15.5, but confirmed the presence of hypoplastic renal tissue or a hypoplastic bi-lobed kidney (Fig. 1C′ and C″). Analysis of kidney volume and nephron number (performed by volumetric analysis of PAS-stained serial kidney sections and WT1 immunostaining) demonstrated a 53% decrease in volume ($n = 11$, $P = 0.0074$) and a 43% decrease in nephron number ($n = 11$, $P<0.0001$) in $Gli3^{\Delta699/\Delta699}$ embryos compared with WT controls. Qualitative analysis of glomeruli, identified by WT1, demonstrated comparable morphology between mutant and control kidneys (data not shown). Together, these data demonstrate murine urogenital system phenotypes consistent with those observed in humans with PHS.

GLI3R impairs caudal nephric duct patterning and uretero-vesicular insertion

Next, we investigated the embryologic mechanisms underlying hydroureter in $Gli3^{\Delta699/\Delta699}$ mice. Our published work using intrapelvic dye injections demonstrated continuity between the renal pelvis and ureter (14). Here, we analyzed the continuity between the ureter and the bladder in mice expressing both the *Hoxb7-Cre* and *Rosa26lacZ* reporter alleles (*Hoxb7-Cre;Rosa26lacZ; Gli3^{\Delta699/ \Delta699}* referred to here as *Gli3^{\Delta699/ \Delta699};UB^{lacZ}*) such that lacZ is expressed in the ureteric epithelium in a Cre-dependent manner. In controls at E16.5, ureters inserted bilaterally into the bladder at the trigone (Fig. 2A). In contrast, mutant mice demonstrated blind-ended ureters (Fig. 2A′, outlined in red) that failed to reach the bladder. Qualitative analysis of *Gli3^{\Delta699};UB^{lacZ}* urogenital ridges harvested at E12.5 revealed a shortened ureter that failed to maintain position with the caudal-most portion of the nephric duct at an embryological stage when the distal ureter is expected to be abutting the cloaca (Fig. 2B and B′, asterisk). In support of this observation, quantitation of the position of the ureteric stalk relative to the tip of the common nephric duct at E11.5 revealed that the distance between the ureteric bud site and the tip of the CND was 56.9% ($P = 0.004$) longer in mutants with no significant difference in overall nephric duct length. Moreover, nuclear fast-red staining of *Gli3^{\Delta699};UB^{lacZ}* histologic sections at E10.5 demonstrated abnormal CND morphology in mutant mice (Fig. 2C–D′, arrowheads). Together, these data demonstrate that GLI3R antagonizes caudal positioning of the ureteric bud site along the nephric duct consistent with a ureteric insertional defect in the bladder.

GLI3R inhibits ureteric bud outgrowth

The appearance of a bi-lobed kidney in a subset of $Gli3^{\Delta699/\Delta699}$ mutant mice suggested a possible abnormality of ureteric budding that produced a double collecting system. We investigated this possibility in E11.5 $Gli3^{\Delta699/\Delta699}$ embryos carrying the *Hoxb7-Cre* and *Rosa26^{lacZ}* alleles. Whole-mount imaging of the urogenital ridge in *Hoxb7-Cre;Rosa26^{lacZ/+};Gli3^{\Delta699/\Delta699}* mice demonstrated a thin and short ureteric stalk with relatively normal looking ureteric tips (Fig. 2E′). Further, a 'Y'-shaped collecting system was observed unilaterally in four of six urogenital ridges imaged (Fig. 2E′). To define the morphologic events that give rise to this Y-shaped collecting system, ureteric budding was analyzed in $Gli3^{\Delta699/\Delta699}$ mice in which expression of *Rosa26^{tdTomato}* was controlled by *Hoxb7-Cre*. Ureteric outgrowth was imaged in urogenital cultures established at E10.5 using real-time fluorescent microscopy. Nephric ducts were live imaged every 5 min over a 48 h period. In *Hoxb7-Cre;Rosa26^{tdTomato/+};Gli3^{+/+}* control mice, the nascent ureteric bud was located caudally, elongated and the elongated ureteric stalk bifurcated into a T-shaped structure (Fig. 3A–D, Supplementary Material, Movie S1). In contrast, in *Hoxb7-Cre;Rosa26^{tdTomato/+};Gli3^{\Delta699/\Delta699}* mice, the nascent ureteric bud outgrowth appeared misshapen, had no caudal bias and was slow growing (Fig. 3A′–D′, Supplementary Material, Movie S2). Surprisingly, in mutant mice, the ureteric bud tips began to branch to form a T-shaped structure before the ureteric stalk had sufficiently elongated (Fig. 3C′). The resulting tips invaded the metanephric mesenchyme at an angle causing a Y-shaped collecting system rather than a 'T' shape (Fig. 3D′). The resulting branch generation remained extra-metanephric giving the appearance of two collecting systems that ultimately converge into one ureteric stalk consistent with the double collecting system phenotype observed in later-staged embryos.

To investigate mechanisms that could explain abnormal ureteric induction in $Gli3^{\Delta699/\Delta699}$ mice, we analyzed cell proliferation, apoptosis and gene expression. The proliferative index of ureteric bud cells, assessed by immunofluorescence for pHH3 and cytokeratin using midsagittal tissue sections generated at
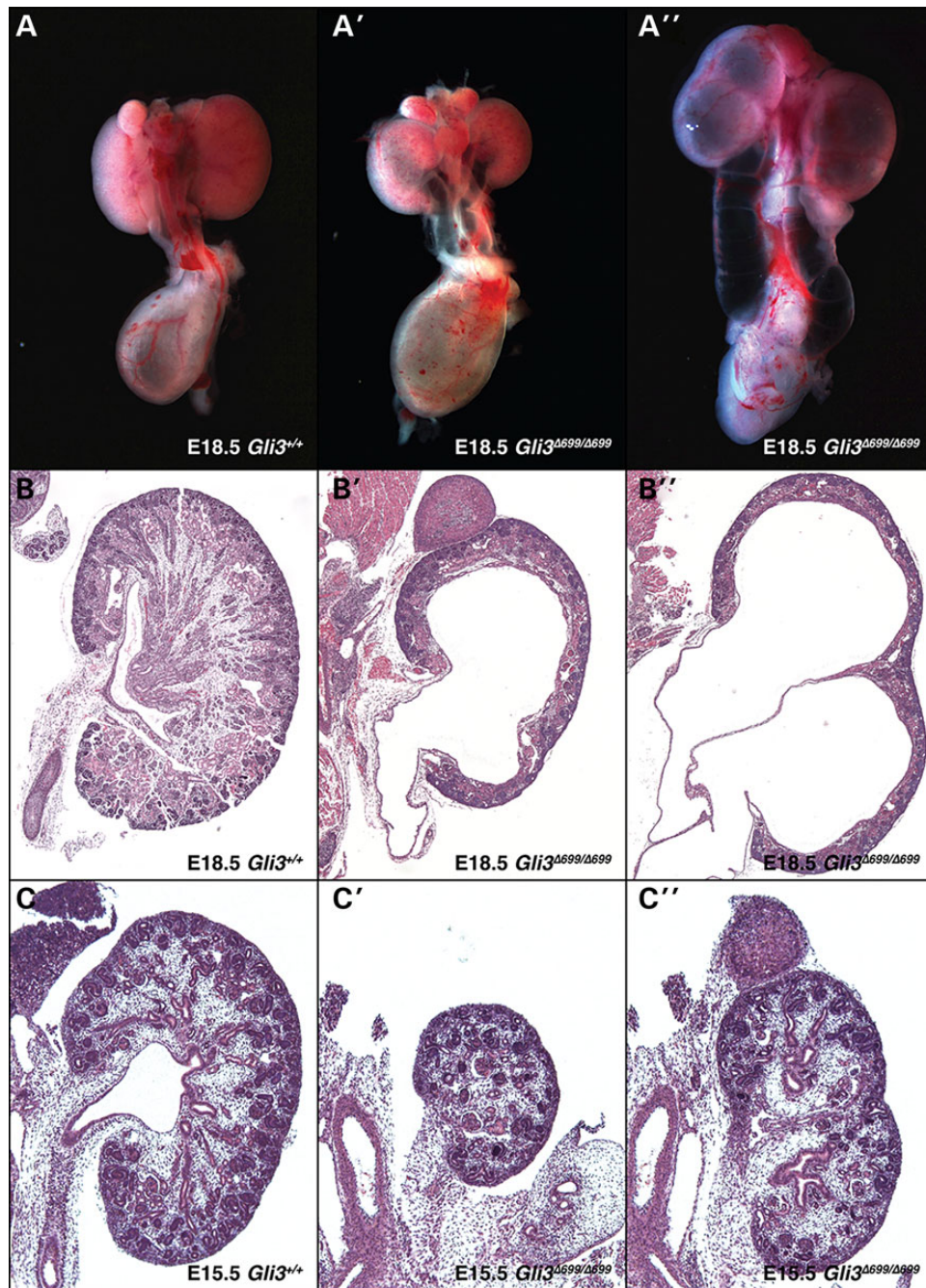
Figure 1. Whole-mount $Gli3^{\Delta699/\Delta699}$ (**A′** and **A″**) urogenital systems at E18.5 demonstrate marked hydroureter and hydronephrosis compared with in $Gli3^{+/+}$ (**A**) controls. H&E tissue sections of $Gli3^{\Delta699/\Delta699}$ (**B′** and **B″**) kidneys demonstrate marked dilation of the kidney, renal hypoplasia (B′) and a duplicated collecting system (B″) in a subset of kidneys when compared with controls (**B**). Hydroureter and hydronephrosis was absent at E15.5 in $Gli3^{\Delta699/\Delta699}$ (**C′** and **C″**) kidney tissue sections; however, they were still marked by renal hypoplasia (C′) and a duplicated collecting system (C″) in a subset of kidneys when compared with controls (**C**).

E11.5, did not differ between mutant and control mice ($n = 7$, data not shown). Moreover there was no evidence of ureteric apoptosis as indicated by activated caspase-3 staining ($n = 7$). Since it has been suggested that a pre-inductive burst of cell proliferation in the nephric duct determines the complement of cells that comprise the ureteric bud (18), we analyzed cell proliferation in this domain at E10.5 using pHH3 and E-cadherin-stained sections. Our results indicate that the proliferative index in the ND at the ureteric bud site was not significantly different between $Gli3^{\Delta699/\Delta699}$ and control mice ($n = 5$, $P = 0.1469$).

To investigate the possible effect of GLI3R expression on the signaling network required for ureteric bud induction and outgrowth, we analyzed expression of *Gdnf, Ret, Wnt11* and their downstream transcriptional targets by whole-mount *in situ* hybridization (Supplementary Material, Fig. S1A–E′). Considering the difference in metanephric size, the expression of *Gdnf, Ret, Wnt11, Etv4* and *Etv5* was not significantly altered in $Gli3^{\Delta699/\Delta699}$ mice at E11.5. Further, lack of perturbation in the expression of *Osr1* confirmed that GLI3R does not alter the size of the metanephric domain (Supplementary Material,
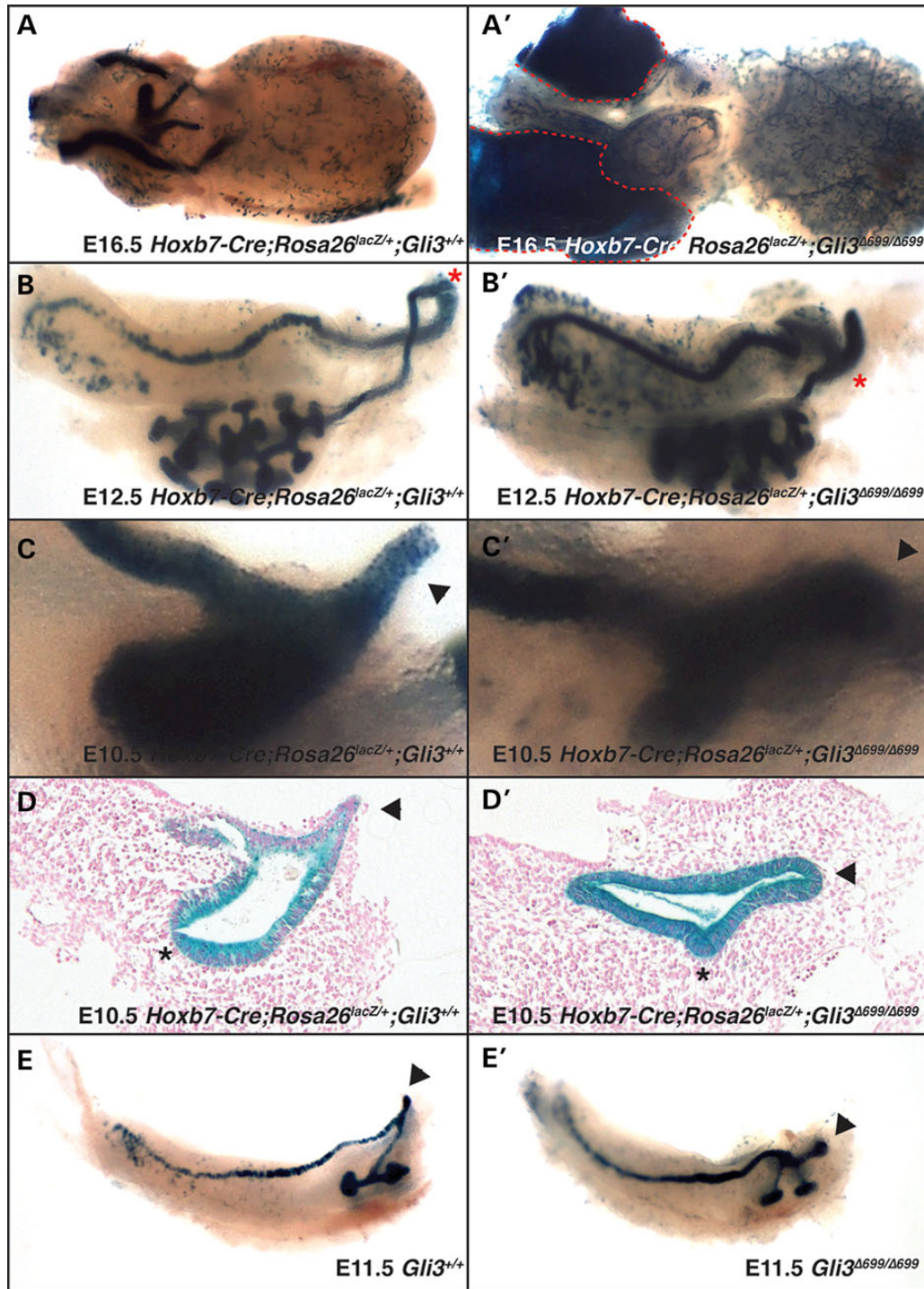
Figure 2. The presumptive ureter inserts into the bladder at E16.5 in *Hoxb7-Cre;Rosa26$^{lacZ/+}$;Gli3$^{+/+}$* (**A**) control mice (visualized in blue). In contrast, the ureter ends blindly and fails to reach the bladder and is highly distended in *Hoxb7-Cre;Rosa26lacZ;Gli3$^{\Delta699/\Delta699}$* (**A'**) mutant mice (visualized in blue, ureter outlined in red). The origin of the ureteric bud is shifted cranially along the common nephric duct (**B'**, asterisk) at E12.5 in *Hoxb7-Cre;Rosa26lacZ;Gli3$^{\Delta699/\Delta699}$* embryos when it normally abuts the tip of the common nephric duct as seen in *Hoxb7-Cre;Rosa26$^{lacZ/+}$;Gli3$^{+/+}$* controls (**B**). At E10.5, the tip of the common nephric duct is pointed in *Hoxb7-Cre;Rosa26$^{lacZ/+}$;Gli3$^{+/+}$* (**C**, arrowhead) control mice but round and misshapen in *Hoxb7-Cre;Rosa26lacZ;Gli3$^{\Delta699/\Delta699}$* mutants (**C'**, arrowhead). The morphology of the common nephric duct is demonstrated in control (**D**) and mutant (**D'**) mice. In a subset of *Hoxb7-Cre;Rosa26lacZ;Gli3$^{\Delta699/\Delta699}$* mutant mice (**E'**), a 'Y'-shaped collecting system is observed with two distinct ureteric buds.

Fig. S1F and F'). Together, these data suggest that GLI3R controls ureteric bud induction and outgrowth via mechanisms independent of cell number control and the *Gdnf–Ret–Wnt11* axis.

GLI3R suppresses an embryonic caudal domain of HH signaling

To assess the state of HH signaling activity that could contribute to the nephric duct patterning defects observed in the *Gli3$^{\Delta699}$*
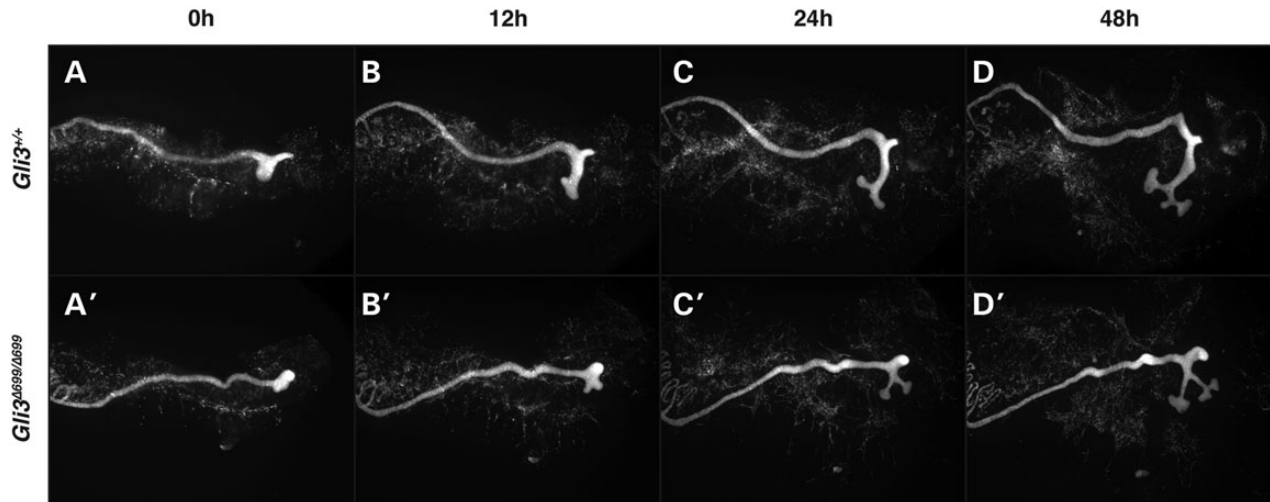
Figure 3. E10.5 tdTomato expressing fluorescent nephric ducts were imaged every 5 min over a 48 h window demonstrating abnormal ureteric budding and stalk elongation in *Hoxb7-Cre;Rosa26$^{tdTomato/+}$;Gli3$^{Δ699/Δ699}$* mutants (**A′–D′**, Supplementary Material, Movie S2) when compared with *Hoxb7-Cre;Rosa26$^{tdTomato/+}$;Gli3$^{+/+}$* controls (Supplementary Material, Movie S1).

model, the *Ptc1^{lacZ}* allele was crossed into the *Gli3^{Δ699}* genetic background to generate *Gli3$^{Δ699/Δ699}$;Ptc1$^{lacZ/+}$* and *Gli3$^{+/+}$;Ptc1$^{lacZ/+}$* embryos. Here, the state of HH signaling is indicated by *Ptc1^{lacZ}* activity. Transverse lacZ-stained tissue sections, generated from E11.5 embryos, demonstrated the domain of HH signaling (Fig. 4A and B). LacZ expression was observed in the gut tube (Fig. 4A and A′, asterisk) that lies along the ventral midline as well as the notochord and adjacent mesenchyme along the dorsum of the embryo (Fig. 4A and A′, arrowhead) in both *Gli3$^{Δ699/Δ699}$; Ptc1$^{lacZ/+}$* and *Gli3$^{+/+}$;Ptc1$^{lacZ/+}$* embryos. However, the intensity of lacZ expression was reduced in *Gli3$^{Δ699/Δ699}$;Ptc1$^{lacZ/+}$* embryos, indicating that HH signaling is attenuated (Fig. 4A and A′). Notably, HH signaling activity was not detected in the nephric duct (Fig. 4C and C′, arrowhead) or nascent ureteric bud (Fig. 4D and D′, arrowhead) in *Gli3$^{Δ699/Δ699}$;Ptc1$^{lacZ/+}$* and *Gli3$^{+/+}$;Ptc1$^{lacZ/+}$* embryos suggesting that these structures are naturally devoid of HH signaling activity at this embryonic stage. In more caudal transverse sections (Fig. 4B and B′) that spanned the common nephric duct, cloaca and vesicular mesenchyme, robust HH signaling activity was detected in *Gli3$^{+/+}$;Ptc1$^{lacZ/+}$* embryos. In contrast, HH signaling activity was markedly reduced in this domain in *Gli3$^{Δ699/Δ699}$; Ptc1$^{lacZ/+}$* embryos (Fig. 4E′ and F′). Together, these results identify the midline metanephric mesenchyme, common nephric duct, cloaca and vesicular mesenchyme as HH signaling domains that are disrupted by obligate GLI3R expression.

GLI3R acts autonomously in the ureteric cell lineage to decrease renal branching morphogenesis

*Gli3$^{Δ699/Δ699}$*mice are characterized by renal hypoplasia and decreased nephron number. Nephron number is determined, in part, by the number of ureteric branches generated during the process of branching morphogenesis (19). Accordingly, we analyzed the effect of GLI3R on this process in a cell-lineage-specific manner. Mice carrying the UB-specific *Hoxb7-Cre* allele or the nephrogenic mesenchyme-specific *Six2-Cre* allele were bred with mice containing the *Rosa26^{Gli3TFLAG}* allele (*Cre*-dependent expression of GLI3R from the ubiquitously expressed *Rosa26* locus) to generate *Hoxb7-Cre;Rosa26$^{Gli3TFLAG/+}$* (UB^{GLI3R}) or *Six2-Cre; Rosa26$^{Gli3TFLAG/+}$* (NM^{GLI3R}) embryos. Ureteric branch number was quantified in tissue isolated at E12.5 from *Gli3$^{Δ699/Δ699}$*

(Fig. 5B), UB^{GLI3R} (Fig. 5C) and NM^{GLI3R} (Fig. 5E) mice. Branching was decreased by 51% ($n = 8$, $P > 0.0001$) in *Gli3$^{Δ699/Δ699}$* kidneys and 47% ($n = 7$, $P = 0.0002$) in UB^{GLI3R} kidneys (Fig. 5F). In contrast, no decrease was detected in NM^{GLI3R} mutants ($n = 4$, $P = 0.125$, Fig. 5E). A single allele of *Gli3^{Δ699}* in UB^{GLI3R} mutants did not further decrease branching morphogenesis (Fig. 5D). Taken together, these data demonstrate that GLI3R in the ureteric cell lineage inhibits renal branching morphogenesis.

GLI3R acts autonomously in the metanephric mesenchyme to control nephron number

Since GLI3R is expressed in all renal cell types in *Gli3$^{Δ699/Δ699}$* kidneys, it is possible that reduced branching morphogenesis does not fully explain the deleterious effects of GLI3R on nephron number. Thus, we investigated whether GLI3R affects the process of nephrogenesis after the point of metanephric induction by ureteric bud tips. Nephrogenesis was examined in *Gli3$^{Δ699/Δ699}$* kidneys using immunostained tissue sections. At E15.5, all intermediate nephrogenic structures (vesicles, comma- and S-shaped) were equally reduced by 48 ± 5% in *Gli3$^{Δ699/Δ699}$* kidneys (Fig. 6F). Next, we determined if GLI3R acts directly in the metanephric mesenchyme to control nephrogenesis and nephron number. GLI3R was conditionally expressed using the nephrogenic mesenchyme-specific *Six2-Cre* allele (*Six2-Cre;Rosa26$^{Gli3TFLAG/+}$*, referred to as NM^{GLI3R}). At E15.5, NM^{GLI3R} kidneys were hypoplastic (Fig. 6A and A′). Cells expressing GLI3R, marked using an anti-FLAG antibody, constituted 49.4 and 89.8% of the SIX2-positive population at E13.5 and E15.5, respectively (Fig. 6B and C). At E15.5, the number of SIX2-positive cells was decreased and the distribution of cells was irregular and discontinuous in NM^{GLI3R} mutants (Fig. 6C). Since nephrogenesis is dependent on Six2-positive cell self-renewal, we measured SIX2-positive cell proliferation using anti-pHH3 and anti-SIX2 (Fig. 6D and D′). At E15.5, the proliferative index was reduced by 69.4% ($n = 10$, $P = 0.0042$, Fig. 6E). There was no evidence of apoptosis as indicated by activated caspase-3 staining (data not shown). These data indicate that obligate GLI3R in the nephrogenic mesenchyme inhibits nephrogenic mesenchyme self-renewal. Despite the decrease in SIX2-positive cell number, FLAG-positive cells were found in all nephrogenic structures and mature glomeruli (Fig. 6C, arrowheads), demonstrating that
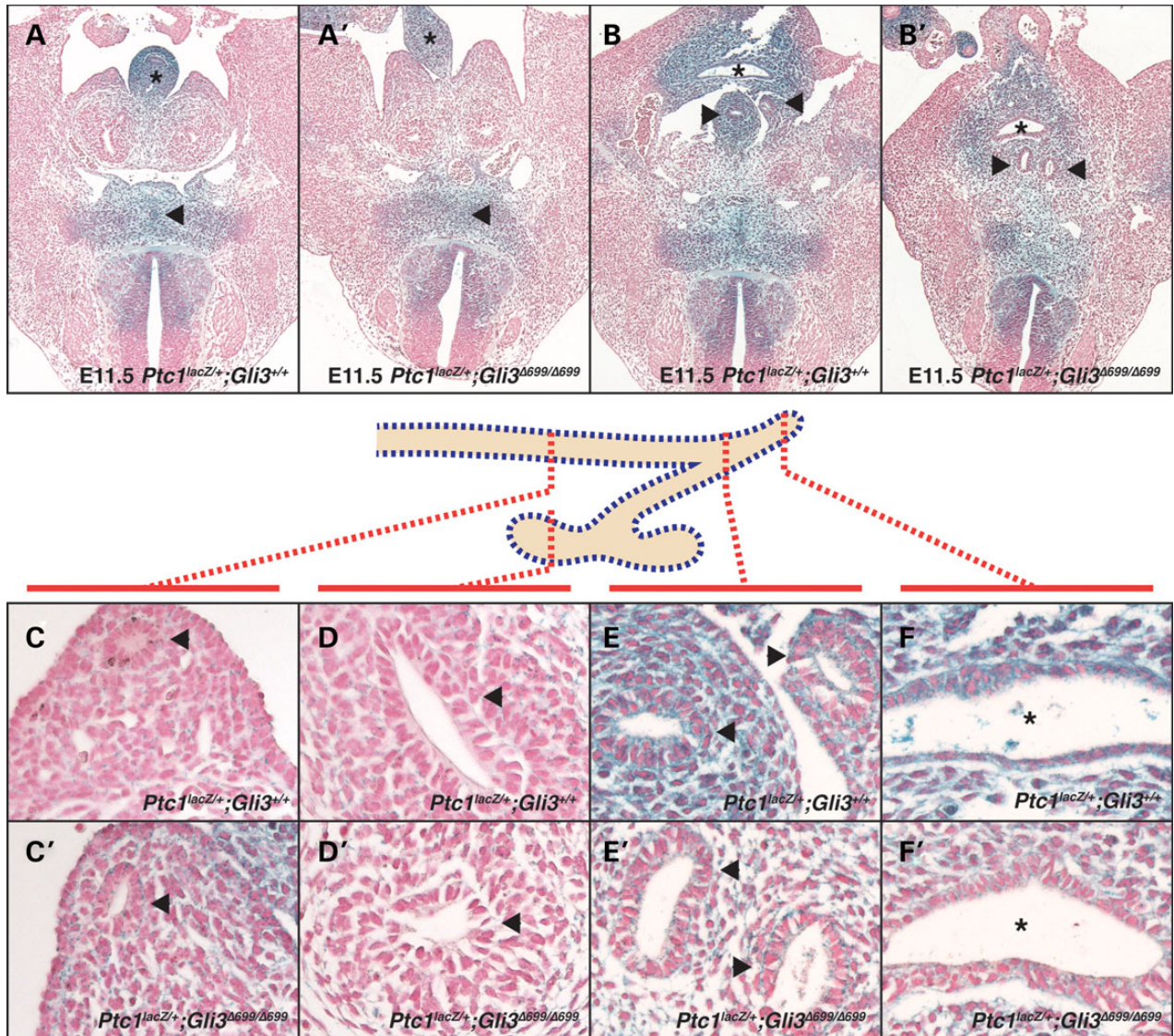
Figure 4. At E11.5, lacZ staining demonstrates the state of Hedgehog signaling in *Gli3*$^{+/+}$;*Ptc1*$^{lacZ/+}$ and *Gli3*$^{\Delta699/\Delta699}$;*Ptc1*$^{lacZ/+}$ transverse tissue sections. LacZ staining is detected in controls in the area surrounding the notochord (**A**, arrowhead), ventral gut tube (**A**, asterisk) and cloaca (**B**, asterisk). LacZ staining is reduced in *Gli3*$^{\Delta699/\Delta699}$; *Ptc1*$^{lacZ/+}$ mutant embryos (**A′** and **B′**, arrowhead, asterisk). No lacZ staining is detected in control and mutant nephric ducts (**C** and **C′**, arrowheads) or ureteric buds (**D** and **D′**, arrowheads). Marked lacZ staining is detected in controls in the common nephric ducts (**E**, arrowheads), cloaca and vesicular mesenchyme (**F**, asterisk) that is reduced in mutants (**E′**, arrowheads, **F′**, asterisk).

GLI3R-expressing cells can contribute to all stages of nephrogenesis. Further, consistent with the observed equivalent decrease in nephrogenic structures in *Gli3*$^{\Delta699/\Delta699}$ mice, intermediate nephrogenic structures were also decreased in *NM*^{GLI3R} mice (reduction in number: renal vesicles, 74.8%; comma-shaped bodies, 76.0%; S-shaped bodies, 81.2%). Together, these data show that GLI3R acts within Six2-positive nephrogenic progenitors to decrease their number but does arrest the process of nephrogenesis.

Kidney development is disrupted by GLI3 repressor and not a loss of GLI3 activator

The disruption in *GLI3* in PHS generates a GLI3R and, thus, limits expression of full-length GLI3 which acts as a transcriptional activator. We determined whether the renal phenotypes observed in *Gli3*$^{\Delta699/\Delta699}$ mutants are due to the presence of increased levels of GLI3R or to a loss of full-length GLI3. *Gli3*$^{\Delta699/xtJ}$ embryos were generated and kidneys were harvested at E18.5. Here, the dose of GLI3R is allelically reduced in the absence of transcriptionally active GLI3. Strikingly, *Gli3*$^{\Delta699/xtJ}$ mutant kidneys were phenotypically normal in comparison to *Gli3*$^{+/+}$ and *Gli3*$^{\Delta699/+}$ controls (Fig. 7A–D). These data provide compelling evidence that kidney development is sensitive to the levels of GLI3R and not to those of full-length GLI3.

Discussion

Development of the permanent mammalian kidney is a complex and highly integrated process that occurs between multiple cell lineages and involves ureteric induction, renal branching morphogenesis and nephrogenesis. Our lab has previously identified a requirement for HH-GLI signaling during kidney induction that is dependent upon levels of the transcriptional repressor GLI3R
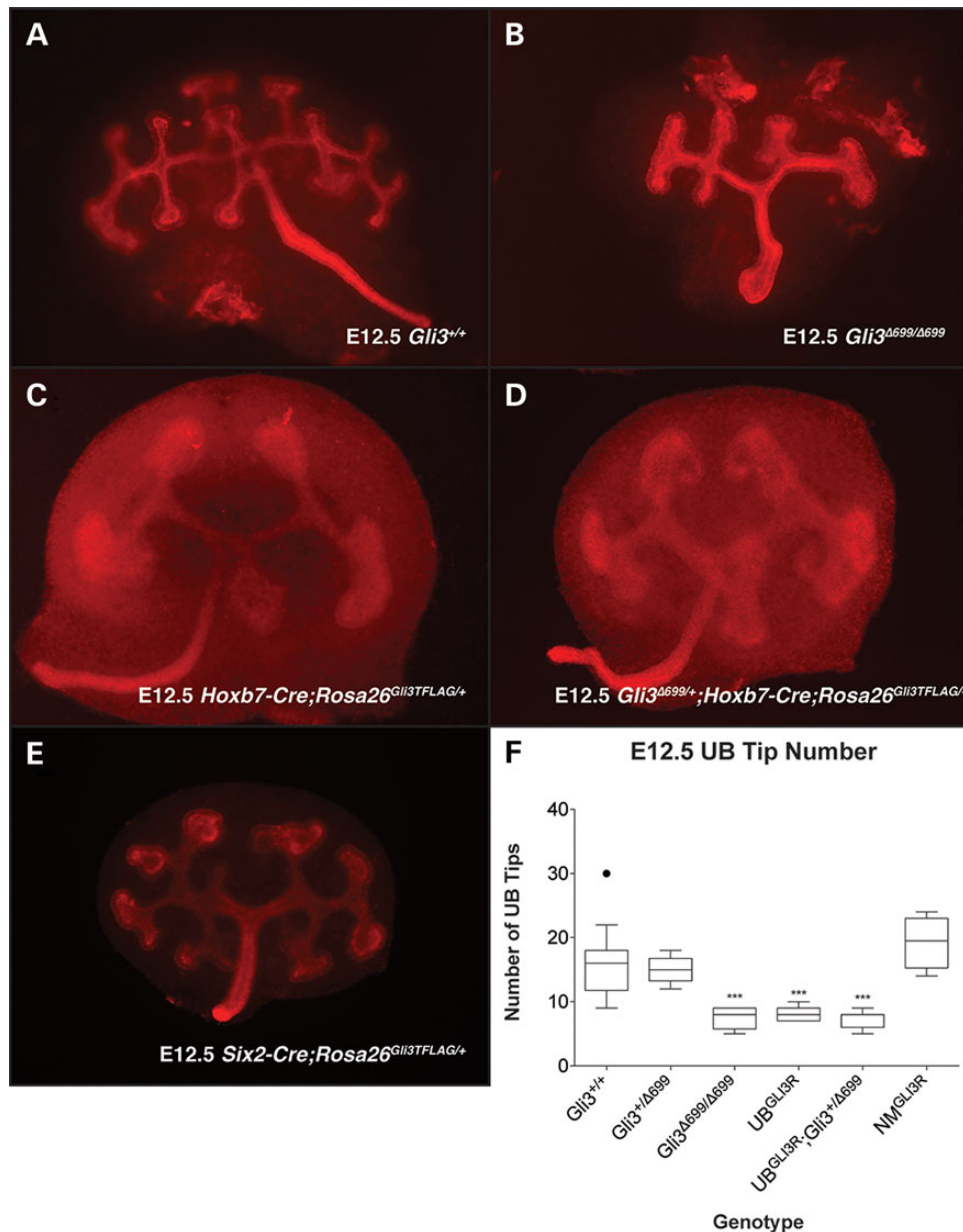
Figure 5. Ureteric branches were visualized at E12.5 by cytokeratin or E-cadherin whole-mount immunofluorescence in control *Gli3*$^{+/+}$(**A**) and mutant *Gli3*$^{\Delta699/\Delta699}$ (**B**), *Hoxb7-Cre;Rosa26*$^{Gli3TFLAG/+}$(**C**), *Hoxb7-Cre;Rosa26*$^{Gli3TFLAG/+}$;*Gli3*$^{\Delta699/+}$ (**D**) and *Six2-Cre;Rosa26*$^{Gli3TFLAG/+}$ (**E**) kidneys. Ureteric tip number was quantified (**F**). Mutant *Gli3*$^{\Delta699/\Delta699}$ (B), *Hoxb7-Cre;Rosa26*$^{Gli3TFLAG/+}$(C) and *Hoxb7-Cre;Rosa26*$^{Gli3TFLAG/+}$;*Gli3*$^{\Delta699/+}$ kidneys had a respective 51% ($n = 8$, $P > 0.0001$), 47% ($n = 7$, $P > 0.0001$) and 50% ($n = 10$, $P > 0.0001$) reduction in branching when compared with controls.

(12). Despite this implication, the GLI3-dependent cellular and lineage-specific mechanisms that give rise to the variety of urinary tract-associated phenotypes in PHS remained unclear.

Detailed study of the *Gli3*$^{\Delta699}$ mouse model and accompanying lineage-specific GLI3R expression models, described here demonstrate that obligate GLI3R impairs ureteric induction and renal branching morphogenesis by impeding ureteric stalk outgrowth (Fig. 8A and A′). Delayed ureteric stalk outgrowth results in renal hypoplasia, duplication of the renal collecting system and hydroureter and hydronephrosis. Reduced branching morphogenesis is specifically caused by GLI3R in the ureteric epithelium at E11.5 and onward leading to a marked reduction in ureteric tip number (Fig. 8C and C′). Canonical branching signaling pathways remain intact at the onset of reduced ureteric branching, suggesting that GLI3R controls a novel and unique subset of genes required for branching morphogenesis. Given the spatial differences in HH signaling within the kidney, it is likely that GLI3R specifies genetic programs unique to the ureteric tip domain at the expense of the ureteric stalk domain. If this is true, then a differential analysis of the genetic profile found in ureteric tip cells and ureteric stalk cells is likely to reveal GLI3R-dependent signaling cascades.

Nephron formation is a complex and highly integrated process that depends on multiple signaling events across a number of distinct pathways. Nephrons derive from the nephrogenic mesenchyme as a pool of self-renewing multipotent cells that are dependent on SIX2 expression. The data presented here demonstrate that GLI3R controls nephrogenic mesenchyme self-
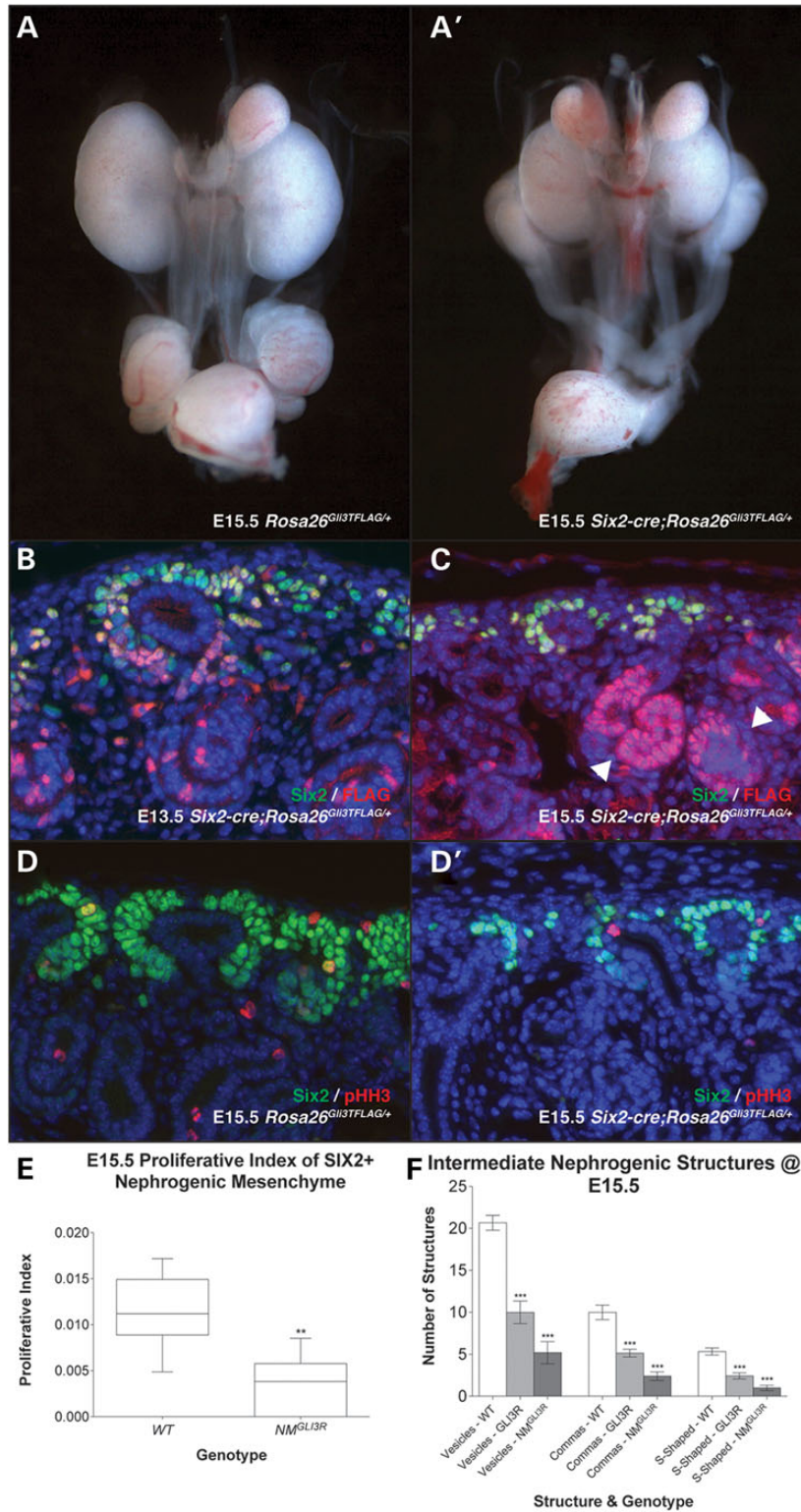
Figure 6. *Six2-Cre;Rosa26Gli3TFLAG/+* mutant (**A′**) kidneys were hypoplastic at E15.5 when compared with *Rosa26*^{Gli3TFLAG/+}controls (**A**). Immunofluorescence for SIX2 and FLAG demonstrate the degree of recombination at E13.5 (**B**) and at E15.5 (**C**) in *Six2-Cre;Rosa26*^{Gli3TFLAG/+} mutants. SIX2-positive nephrogenic mesenchyme caps were irregular and sparse in *Six2-Cre;Rosa26*^{Gli3TFLAG/+} mutants (**C** and **D′**) at E15.5 when compared with controls (**D**). FLAG-positive cells are found in nephrogenic structures (**C**, arrowheads). Proliferation was assessed at E15.5 by anti-pHH3 staining and found to be reduced by 69.4% (**E**). Renal vesicles, comma-shaped bodies and S-shaped bodies were reduced by 48.4, 51.4 and 45.6% in *Gli3*^{Δ699/Δ699} mutant kidneys and by 74.8, 76.0 and 81.2% in *Six2-Cre;Rosa26*^{Gli3TFLAG/+} mutant kidneys.

renewal in a *Six2*-independent manner (Fig. 8B and B′). It remains unclear if GLI3R acts in parallel with or downstream of *Six2* to control this self-renewal process. Although the renal cortex does not have an active HH signaling domain, these data demonstrate that the nephrogenic mesenchyme is indeed sensitive to increased levels of GLI3R.
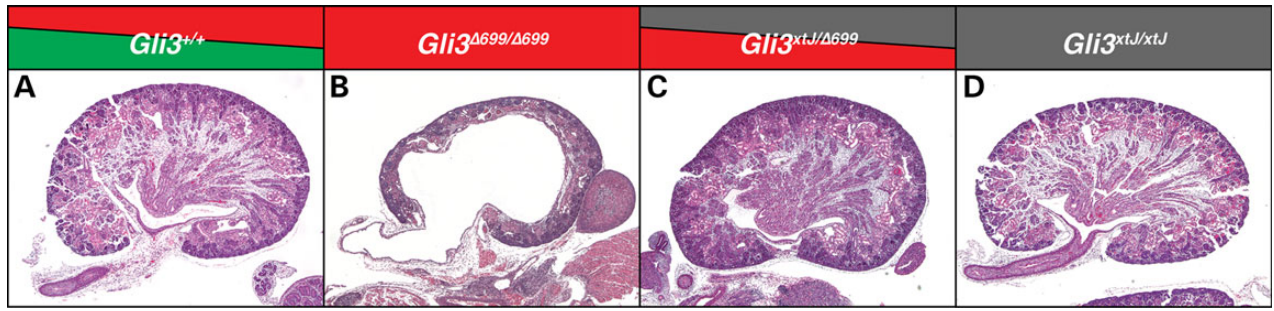
Figure 7. A single allele of *Gli3*$^{\Delta 699}$ was replaced with a null *Gli3*^{xtJ} allele in *Gli3*$^{\Delta 699/\Delta 699}$ mutants. In contrast to *Gli3*$^{\Delta 699/\Delta 699}$ mutant kidneys at E18.5 (**B**), *Gli3*$^{\Delta 699/xtJ}$ mutant kidneys (**C**) are phenotypically normal and resemble *Gli3*$^{+/+}$ control kidneys (**A**). *Gli3*$^{xtJ/xtJ}$ kidneys are shown for comparison (**D**).
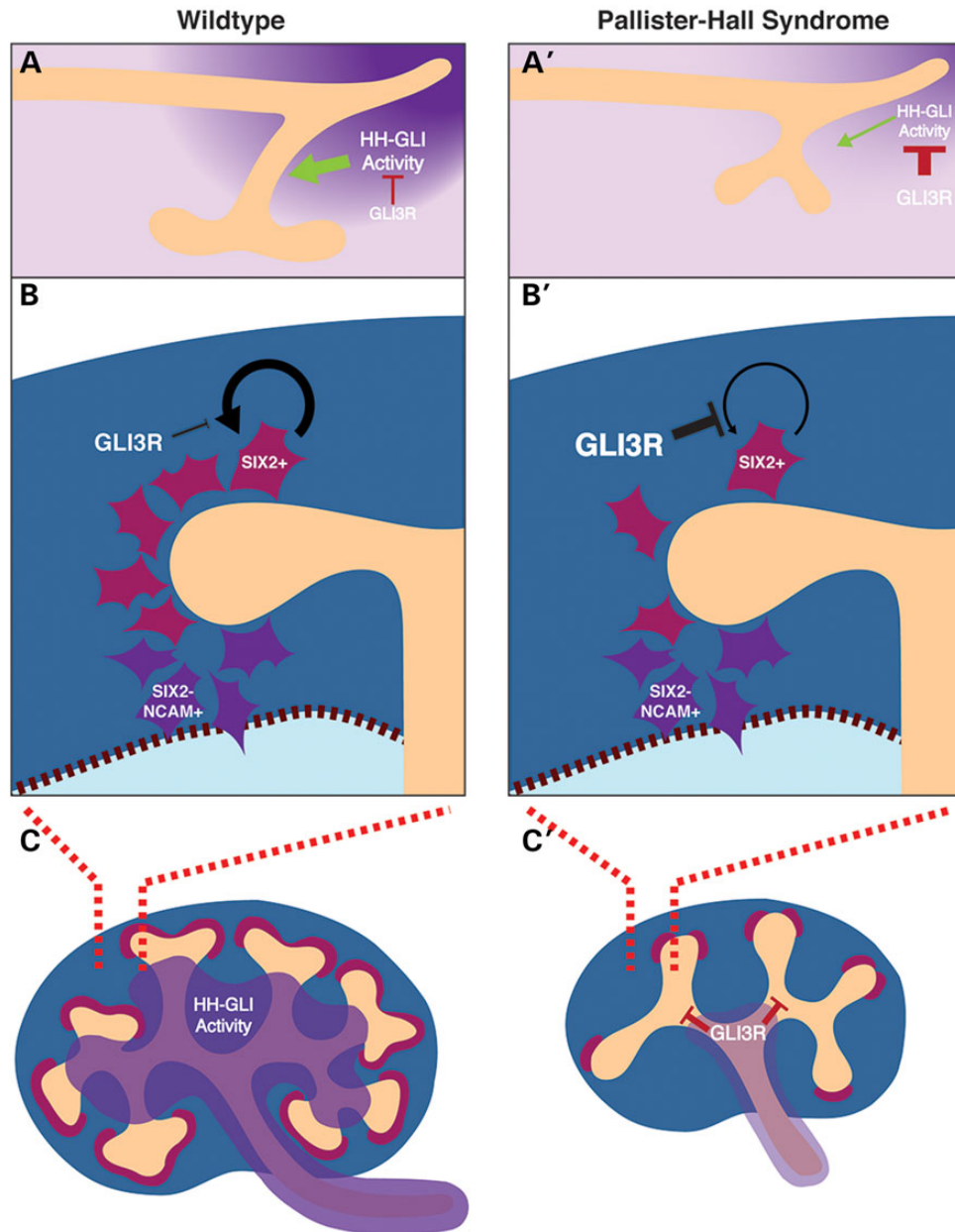

Figure 8. A model is presented whereby GLI3R inhibits HH signaling activity in the caudal nephric duct that is required for ureteric outgrowth (**A** and **A'**). When GLI3R is ectopically activated in the nephrogenic mesenchyme, nephrogenic mesenchyme self-renewal is inhibited (**B** and **B'**) leading to a nephron deficit. Finally, when GLI3R is ectopically activated in the ureteric bud lineage, branching morphogenesis is inhibited (**C** and **C'**) leading to renal hypoplasia.

The severity of GLI3 mutations found in PHS patients is believed to be associated with the severity of disease phenotype (2,3). Here we demonstrate, using germline mouse models, that urogenital system development is sensitive to the levels of GLI3R but not to full-length GLI3 in contrast to limb development that is impaired by a loss of full-length GLI3 (20). Interestingly, genetic reduction in the mouse $Gli3^{\Delta699}$ allele to hemizygosity restores kidney development. Recent evidence suggested that the terminal amino-acid sequence produced by the $Gli3^{\Delta699}$ allele reduces the potency of the peptide product (21). This observation may explain the autosomal recessive nature of the $Gli3^{\Delta699}$ PHS model presented here. Serendipitously, the reduced potency of the $Gli3^{\Delta699}$ allele has facilitated a more detailed analysis of the specific processes disrupted by obligate GLI3R in the developing kidney. Expression of the $Rosa26^{Gli3TFLAG}$ allele, used here to investigate the cell-lineage-specific effects of GLI3R, generated phenotypes in the ureteric and nephrogenic lineages. Since the relative potency of the $Rosa26^{Gli3TFLAG}$ allele compared with PHS mutations is unknown, it remains unclear whether the severity of the phenotypes observed in lineage-specific $Rosa26^{Gli3TFLAG}$ models phenocopies many of the renal–urinary pathologies in PHS.

Urogenital system malformations have been reported in PHS cases and are marked by hydroureter, hydronephrosis and a common urogenital opening (2,3,6). Consistent with these findings, our data demonstrate that GLI3R disrupts caudal nephric duct patterning by altering the ureteric bud site relative to the distal tip of the nephric duct. Our data also illustrate a previously undefined HH signaling domain at E11.5 in the caudal nephric duct and adjacent mesenchyme that is sensitive to the levels of GLI3R. Indeed, other more distal elements of the urinary tract including the bladder are sensitive to HH signaling levels during embryogenesis (22,23). When HH signaling is abrogated by a temporal deletion of *Shh*, a population of peri-cloacal mesenchyme is lost that leads to hydroureter and hydronephrosis (22). Known HH responsive effectors of bladder development include genes responsible for smooth muscle differentiation (16,23,24). Connectivity between the CND and bladder is established in part by the transcription factor *Gata3* in an RET-dependent fashion (25). We have shown that *Ret* expression in a germline model of PHS is unperturbed, suggesting that HH signaling may act via a novel mechanism to control CND patterning and vesicular insertion. It remains unclear whether the CND is competent in a germline model of PHS to establish continuity with the cloaca or whether there is a defect inherent to the cloaca that inhibits CND invasion.

Our findings demonstrate the contributions of GLI3R to the developing renal–urinary system in germline and lineage-specific models of PHS. We conclude that GLI3R alters the normal HH signaling domain in the caudal embryo, and that GLI3R impairs nephric duct patterning, renal branching morphogenesis and nephrogenic mesenchyme self-renewal. Whereby some non-renal features of PHS are caused by a loss of full-length GLI3, we conclude that urogenital system development in PHS is dependent on increased levels of GLI3R. Our findings provide novel insight into the embryological origins of the pathologies found in renal–urogenital systems in PHS.

Materials and Methods
Animals

The $Gli3^{\Delta699}$ mouse line was previously described (10) and maintained on a mixed C57Bl6 background. The *Hoxb7-Cre* (26) (UB) and *Six2-Cre* (27) (NM) mouse lines were previously described and maintained on a mixed background. The $Rosa26^{Gli3TFLAG}$ allele was previously described, and homozygotes were maintained on an inbred C57Bl6 background. The $Rosa26^{lacZ}$ allele was previously described, and homozygotes were maintained on an outbred CD1 background. The $Rosa26^{tdTomato}$ allele was previously described, and homozygotes were maintained on an inbred C57Bl6 background. All animals were used in accordance with our animal use protocol at the Toronto Centre for Phenogenomics and in compliance with the Canadian Council on Animal Care.

Live culture

E10.5 urogenital ridges were resected in DMEM:F12 + 1% PenStrep (Invitrogen), bisected along the sagittal midline and transferred to 3 μm transwell filter inserts. Ridges were cultured using DMEM:F12 (Invitrogen) + 10% FBS (Gibco) + 1% PenStrep (Invitrogen) for 48 h and imaged every 5 min. Cultures were kept humidified at 37°C in a 5% CO_2 atmosphere with a Pecon XL chamber and Zeiss incubation module fitted to an Axiovert 200 M inverted epifluorescent microscope using AxioVision 4.8 software (Zeiss Canada).

Tissue preparation and histology

Tissue harvested for histology, section immunofluorescence and section *in situ* hybridization was fixed in 4% PFA: PBS overnight at 4°C and dehydrated in 70% ethanol to be processed for paraffin embedding. E10.5 and E11.5 tissue was first embedded in Histogel (Thermo Fisher) to orient the specimen and then subsequently dehydrated and processed for paraffin embedding. Tissue harvested for whole-mount immunofluorescence was fixed using −20°C 4:1 (Methanol:DMSO) Dent's Fix and stored at −20°C until use. Whole tissue harvested for lacZ staining was fixed and washed as previously described and stained for 48 h at 37°C. LacZ-stained tissue was subsequently processed for paraffin embedding and sections were counterstained using nuclear fast red.

Immunofluorescence

Section immunofluorescence was performed on 4 μm paraffin sections as previously described; however, Dako serum-free protein block was used for blocking, primary and secondary incubation buffers. Whole-mount immunofluorescence was performed as previously described. The following antibodies were used: α-Calbindin-D28K (1:100) (Sigma, C9848 and C7354), α-activated Caspase 3 (1:500) (Cell Signaling, 5A1E), α-Cited 1 (1:150) (Neo-Markers, RB-9219-P0), α-pan Cytokeratin (1:100) (Sigma, C2562), α-E-cadherin (1:250) (Cell Signaling, 24E10), α-GFP (1:250) (Rockland, 600–401–215), α-Gli3 (Sigma, 2C9), α-NCAM (1:250) (Sigma, C9672), α-phospho-Histone H3 (1:250) (Cell Signaling, D2C8 & 6G3), α-Sall1 (1:250) (Abcam, ab31526), α-Six2 (1:250) (Proteintech, 11562-1-AP), α-SMA (1:250) (Sigma, A5228), α-RFP (1:250) (Rockland, 600-401-379), α-WT1 (1:250) (Dako, Clone 6F-H2).

RNA *in situ* hybridization

Section and whole-mount RNA *in situ* hybridization was performed as previously described. DIG-labeled riboprobes were made as previously described from PCR linearized plasmid DNA. The following probes were newly generated and sequence verified from E15.5 mouse kidney cDNA (CD-1 background): *Bmp4*, *Raldh2*, *Etv4*, *Etv5*.

Supplementary Material

Supplementary Material is available at *HMG* online.

Acknowledgements

Funding

References

1. Tsanev, R., Tiigimagi, P., Michelson, P., Metsis, M., Osterlund, T. and Kogerman, P. (2009) Identification of the gene transcription repressor domain of Gli3. *FEBS Lett.*, **583**, 224–228.
2. Demurger, F., Ichkou, A., Mougou-Zerelli, S., Le Merrer, M., Goudefroye, G., Delezoide, A.L., Quelin, C., Manouvrier, S., Baujat, G., Fradin, M. *et al.* (2015) New insights into genotype–phenotype correlation for GLI3 mutations. *Eur. J. Hum. Genet.*, **23**, 92–102.
3. McPherson, E. and Cold, C. (2013) Severe Pallister–Hall syndrome with persistent urogenital sinus, renal agenesis, imperforate anus, bilateral hypothalamic hamartomas, and severe skeletal anomalies. *Am. J. Med. Genet. A*, **161A**, 2666–2669.
4. Hall, J.G. (2014) Pallister–Hall syndrome has gone the way of modern medical genetics. *Am. J. Med. Genet. C, Semin. Med. Genet.*, **166C**, 414–418.
5. Hall, J.G., Pallister, P.D., Clarren, S.K., Beckwith, J.B., Wiglesworth, F.W., Fraser, F.C., Cho, S., Benke, P.J., Reed, S.D. and Optiz, J.M. (1980) Congenital hypothalamic hamartoblastoma, hypopituitarism, imperforate anus, and postaxial polydactyly—a new syndrome? Part I: clinical, causal, and pathogenetic considerations. *Am. J. Med. Genet.*, **7**, 47–74.
6. Johnston, J.J., Olivos-Glander, I., Killoran, C., Elson, E., Turner, J.T., Peters, K.F., Abbott, M.H., Aughton, D.J., Aylsworth, A.S., Bamshad, M.J. *et al.* (2005) Molecular and clinical analyses of Greig Cephalopolysyndactyly and Pallister–Hall syndromes: robust phenotype prediction from the type and position of GLI3 mutations. *Am. J. Hum. Genet.*, **76**, 609–622.
7. Pallister, P.D., Hecht, F. and Herrman, J. (1989) Three additional cases of the congenital hypothalamic 'hamartoblastoma' (Pallister–Hall) syndrome. *Am. J. Med. Genet.*, **33**, 500–501.
8. Jamsheer, A., Sowinska, A., Trzeciak, T., Jamsheer-Bratkowska, M., Geppert, A. and Latos-Bielenska, A. (2012) Expanded mutational spectrum of the GLI3 gene substantiates genotype–phenotype correlations. *J. Appl. Genet.*, **53**, 415–422.
9. Narumi, Y., Kosho, T., Tsuruta, G., Shiohara, M., Shimazaki, E., Mori, T., Shimizu, A., Igawa, Y., Nishizawa, S., Takagi, K. *et al.* (2010) Genital abnormalities in Pallister–Hall syndrome: report of two patients and review of the literature. *Am. J. Med. Genet. A*, **152A**, 3143–3147.
10. Bose, J., Grotewold, L. and Ruther, U. (2002) Pallister–Hall syndrome phenotype in mice mutant for Gli3. *Hum. Mol. Genet.*, **11**, 1129–1135.
11. Yu, J., Carroll, T.J. and McMahon, A.P. (2002) Sonic hedgehog regulates proliferation and differentiation of mesenchymal cells in the mouse metanephric kidney. *Development*, **129**, 5301–5312.
12. Hu, M.C., Mo, R., Bhella, S., Wilson, C.W., Chuang, P.-T., Hui, C.-C. and Rosenblum, N.D. (2006) GLI3-dependent transcriptional repression of Gli1, Gli2 and kidney patterning genes disrupts renal morphogenesis. *Development*, **133**, 569–578.
13. Vokes, S.A., Ji, H., Wong, W.H. and McMahon, A.P. (2008) A genome-scale analysis of the cis-regulatory circuitry underlying sonic hedgehog-mediated patterning of the mammalian limb. *Genes Dev.*, **22**, 2651–2663.
14. Cain, J.E., Islam, E., Haxho, F., Blake, J. and Rosenblum, N.D. (2011) GLI3 repressor controls functional development of the mouse ureter. *J. Clin. Invest.*, **121**, 1199–1206.
15. Cain, J.E., Islam, E., Haxho, F., Chen, L., Bridgewater, D., Nieuwenhuis, E., Hui, C.-C. and Rosenblum, N.D. (2009) GLI3 repressor controls nephron number via regulation of Wnt11 and Ret in ureteric tip cells. *PLoS ONE*, **4**, e7313.
16. Caubit, X., Lye, C.M., Martin, E., Core, N., Long, D.A., Vola, C., Jenkins, D., Garratt, A.N., Skaer, H., Woolf, A.S. *et al.* (2008) Teashirt 3 is necessary for ureteral smooth muscle differentiation downstream of SHH and BMP4. *Development*, **135**, 3301–3310.
17. Vokes, S.A., Ji, H., McCuine, S., Tenzen, T., Giles, S., Zhong, S., Longabaugh, W.J.R., Davidson, E.H., Wong, W.H. and McMahon, A.P. (2007) Genomic characterization of Gli-activator targets in sonic hedgehog-mediated neural patterning. *Development*, **134**, 1977–1989.
18. Chi, X., Michos, O., Shakya, R., Riccio, P., Enomoto, H., Licht, J.D., Asai, N., Takahashi, M., Ohgami, N., Kato, M. *et al.* (2009) Ret-dependent cell rearrangements in the Wolffian duct epithelium initiate ureteric bud morphogenesis. *Dev. Cell*, **17**, 199–209.
19. Blake, J. and Rosenblum, N.D. (2014) Renal branching morphogenesis: morphogenetic and signaling mechanisms. *Semin. Cell Dev. Biol.*, **36**, 2–12.
20. Wang, C., Rüther, U. and Wang, B. (2007) The Shh-independent activator function of the full-length Gli3 protein and its role in vertebrate limb digit patterning. *Dev. Biol.*, **305**, 460–469.
21. Cao, T., Wang, C., Yang, M., Wu, C. and Wang, B. (2013) Mouse limbs expressing only the Gli3 repressor resemble those of Sonic hedgehog mutants. *Dev. Biol.*, **379**, 221–228.
22. Haraguchi, R., Matsumaru, D., Nakagata, N., Miyagawa, S., Suzuki, K., Kitazawa, S. and Yamada, G. (2012) The hedgehog signal induced modulation of bone morphogenetic protein signaling: an essential signaling relay for urinary tract morphogenesis. *PLoS One*, **7**, e42245.
23. DeSouza, K.R., Saha, M., Carpenter, A.R., Scott, M. and McHugh, K.M. (2013) Analysis of the Sonic Hedgehog signaling pathway in normal and abnormal bladder development. *PLoS One*, **8**, e53675.
24. Lye, C.M., Fasano, L. and Woolf, A.S. (2010) Ureter myogenesis: putting teashirt into context. *J. Am. Soc. Nephrol.*, **21**, 24–30.
25. Chia, I., Grote, D., Marcotte, M., Batourina, E., Mendelsohn, C. and Bouchard, M. (2011) Nephric duct insertion is a crucial step in urinary tract maturation that is regulated by a Gata3-Raldh2-Ret molecular network in mice. *Development*, **138**, 2089–2097.
26. Zhao, H., Kegg, H., Grady, S., Truong, H.-T., Robinson, M.L., Baum, M. and Bates, C.M. (2004) Role of fibroblast growth factor receptors 1 and 2 in the ureteric bud. *Dev. Biol.*, **276**, 403–415.
27. Kobayashi, A., Valerius, M.T., Mugford, J.W., Carroll, T.J., Self, M., Oliver, G. and McMahon, A.P. (2008) Six2 defines and regulates a multipotent self-renewing nephron progenitor population throughout mammalian kidney development. *Cell Stem Cell*, **3**, 169–181.